J Mater Sci (2007) 42:2486–2491
DOI 10.1007/s10853-006-0462-4

Microtexture and electrical properties of PAN-ACF

Jong Gyu Lee · Je Young Kim · Sung Hyun Kim

Received: 12 August 2005 / Accepted: 17 May 2006 / Published online: 19 November 2006

Abstract Microstructure and electric conductivity of PAN-based activated carbon fibers (PAN-ACF) were investigated using tension and KOH activation. The application of tension during stabilization decreased pore volume as well as specific surface area. Increase of KOH solution concentration caused serious damage to the surface of PAN-ACF. This surface damage of PAN-ACF resulted in increase of specific surface, pore volume and wider pore size distribution. PAN-ACF with higher tension showed higher electric conductivity. However, the electric conductivity was decreased by the increased BET surface area.

Introduction

During the last years, the electrode materials for electric double layer capacitor (EDLC) has been extensively developed [1–3] due to the increasing demand for a new kind of accumulators of electric energy with a high specific power and a long durability. A great interest has been focused on the application of carbons as electrode materials because of their accessibility, an easy processability and relatively low cost. Apart from it, carbon materials are environmentally friendly. They are chemically stable in different solutions (from strongly acidic to basic) and able for performance in a wide range of temperatures.

Theoretically, in order to achieve high specific capacitance, the carbon material of high surface area should be chosen as electrode material. However, the activated carbon manufactured under different conditions may have different porosity and surface conditions. All the BET surface area is not electrochemically accessible. Several authors have observed that there is significant deviation from linearity between BET surface area and specific capacitance at high BET surface area (i.e. >1000 $m^2 g^{-1}$) [4]. This deviation is due to the non-accessibility of all the pores to the electrolyte solution.

Carbon electrode is well polarizable; however, its electric conductivity strongly depends on the thermal treatment, microtexture, surface functional group and content of heteroatom. In the investigation of materials for paste electrodes of EDLC, the conductivity is one of the essential properties. The influence of electric conductivity in the promotion of double layer capacitance has already been suggested for carbon electrode using commercial activated carbon [5], exfoliated carbon fiber [6] and pitch-based carbon fiber [7]. It is well known that the inclusion of conductive filler can greatly alter the dielectric characteristics of the polymer medium in which they are dispersed [8–10].

This study is to investigate the effect of microtexture and surface functional group on the electric conductivity of carbon material with the purpose of selecting materials for the manufacture of porous electrode for EDLC using polyacrylonitrile-based activated carbon fiber (PAN-ACF).

J. G. Lee · J. Y. Kim
Energy Research Team, Research Institute of Science and Technology (RIST), Pohang, Korea

S. H. Kim (✉)
Department of Chemical and Biological Engineering, Korea University, Seoul, Korea
e-mail: kimsh@korea.ac.kr

Methodology

Preparation of the PAN-ACF

The PAN precursor fiber (copolymer, Courtaulds Company) tows containing 12,000 filaments of 1.12 denier were used as a starting material. The stabilized fiber was prepared at 250 °C for 3 h in a forced convection oven. In preparation of the stabilized fiber, various tensions (0, 0.2, 0.6 kgf) were applied to the tows with one end of the fiber fixed and the other end hung with a constant weight. The stabilized fibers were immersed in a 1-mole KOH solution for 1 h, and then filtered and dried. Samples were designated as T081, T281, and T681. The stabilized fibers stained with KOH were crushed using the mixer mill (Retsch M350, Germany). The stabilized fiber applied the highest tension of 0.6 kgf was also immersed in 2 and 3-mole KOH solutions for 1 hour. These samples were designated T682, and T683. The crushed fiber was heat-treated at 800 °C in a nitrogen atmosphere for 1 h and then washed using diluted 0.5 N hydrochloric acid and hot water and finally dried. The ACFs were screened into 38 μm or below by length, and its electric conductivity was measured using the 4-point probe technique.

Nitrogen adsorption isotherms

Nitrogen adsorption isotherms at 77 K were measured using an ASAP 2010 (Micromeritics). Prior to each measurement, the samples were degassed at 573 K for 10 h. The specific surface area of the sample was calculated by the BET model [11]. The pore volume and size were calculated from the adsorbed nitrogen gas volume based on the assumption which liquid nitrogen filled the sample pores at a relative pressure of 0.995. The pore size distribution was calculated using the DFT program provided by Micromeritics.

Measurements of XRD, XPS and SEM

The X-ray diffraction (XRD, RIGAKU, DMXA 1400) measurements were also conducted on the X-ray diffractometer using CuKα-radiation. The surface chemical composition of the sample was analyzed by X-ray photoelectron spectroscopy (XPS). Photoelectron spectra were obtained using photoelectron spectrometer (ESCA Lab-250, VG Scientific) using monochromatic AlKα X-ray radiation (1486.6 eV). The analysis chamber was maintained at lower pressure than 5×10^{-9} Pa. The peak fitting was repeated until an acceptable fit was obtained. The positions of the deconvoluted peaks (binding energy-BE) were determined based on both literature data and empirically derived values.

Measurement of the electric conductivity

The electric conductivities of the samples were measured using the 4-point probe packed-bed technique at room temperature of 25 °C. The measurement setup diagram was shown in Fig. 1. Electric resistance was measured by connecting the voltage/current source (Keithly 228A) and programmable electrometer (Keithly 617) to the copper electrode connected to the top and bottom of the 1 cm-diameter packed-bed made of plastic material. Pressure was applied to the top of the packed bed using a hydraulic press during measurement of the electric resistance of the samples. Electric conductivity $1/\rho$ (1/Ωcm) was derived using the following equation:

$$1/\rho = A/Rl$$

where R, l and A, denote the measured resistance (Ω), sample length (cm) and cross section area of the bed (cm^2) respectively.

Results and discussion

Pore structure of PAN-ACFs

Figure 2 shows the nitrogen adsorption isotherms of the samples. According to the BDDT classification, the

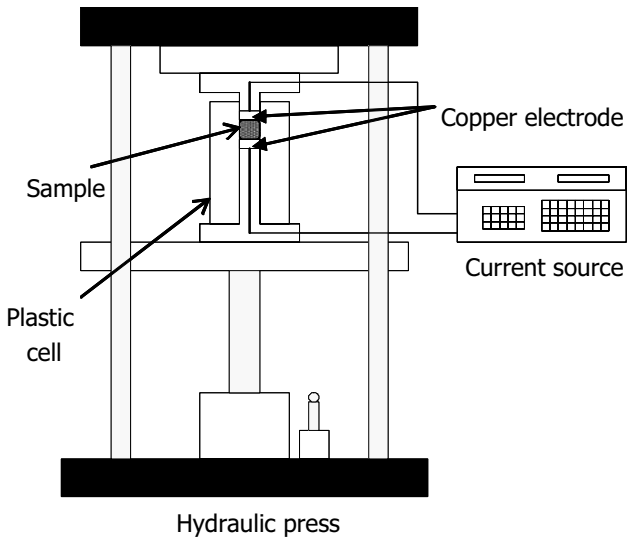

Fig. 1 Apparatus employed to measure the electric resistance of the samples

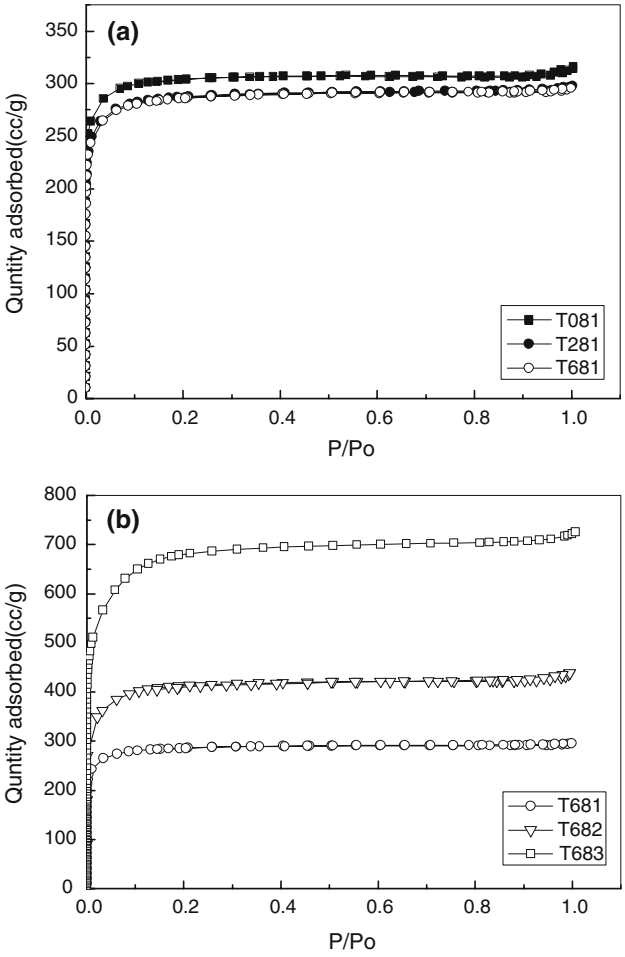

Fig. 2 Adsorption isotherms of N2 of the various samples at 77 K, based on applied tension (**a**) and KOH mol (**b**)

nitrogen adsorption isotherms are typical microporous Type I. Figure 2a shows the nitrogen adsorption isotherms under various tensions of samples. The nitrogen adsorption isotherms for various samples as a function of the mole concentration numbers of KOH solution are shown in Fig. 2b. At low relative pressures, the nitrogen adsorption isotherm of T683 in Fig. 2b appears to have a more rounded ''knee,'' which is normally associated with wide micropore. The isotherms of T683 show a rounded ''knee,'' indicating a wider pore size distribution. After a relative pressure of about 0.2 is reached, there is still a further increase in amount adsorbed with increasing relative pressure, which reflects a certain amount of mesopore volume in T683.

The physical properties of the PAN-ACFs were summarized in the Table 1. The PAN-ACFs had microporous structure. The specific surface area decreases with increasing tension during the stabilization as shown in Table 1. Figure 3 shows the pore size distribution of PAN-ACFs based on the density functional theory (DFT).

As showed in Fig. 3a, the samples show the narrow pore size distribution. The pore volume is observed to decrease under high tension (T681) of 0.6 kgf compared with low tension (T081). The stabilization process in an air atmosphere is the exothermic reaction by the complex molecular motion [12]. The shrinkage would be balanced by elongation under tension. The elongation will excess shrinkage under higher tension. Therefore, the distance between molecules would be decreased. As the tension increase, the pore volume is decreased and leads to the stretching caused by the movement of molecules along with the fiber axis.

The pore size distributions of the samples treated under different KOH mole concentration were plotted in Fig. 3b. T681 shows the narrow pore size distribution. T683 shows the wide pore size distribution, which would be caused by the interaction of potassium and carbon during heat treatment.

X-ray Diffraction (XRD)

Figure 4 shows XRD of the samples given under tension during the stabilization. The inter-planar spacing of T681 was smaller than T081 and T281, because a crystallite was formed from the PAN fiber along with the fiber axis under tension during the stabilization. Conversely, the inter-planar spacing was increased with increasing KOH mole concentration because of

Table 1 Physical properties of the PAN-ACFs

Sample	S^{a}_{BET}(m^2/g)	Pore size (Á)	Pore vol (cm^3/g)	S^{b}_{DFT}(m^2/g)	Elemental analysis by XPS (at%)				
					C1s	N1s	O1s	O/C (%)	N/C (%)
T081	1005	19.1	0.48	977	85	10.2	4.8	5.6	12
T281	953	19	0.45	909	84.6	10.7	4.7	5.5	12.6
T681	935	17.6	0.45	891	84.6	10.9	4.5	5.3	12.8
T682	1380	19.2	0.66	1201	86	10	4	4.6	11.6
T683	2312	19.2	1.11	1734	88	8.2	3.8	4.3	9.32

[a] S_{BET}; specific surface area by BET

[b] S_{DFT}; specific surface area by DFT

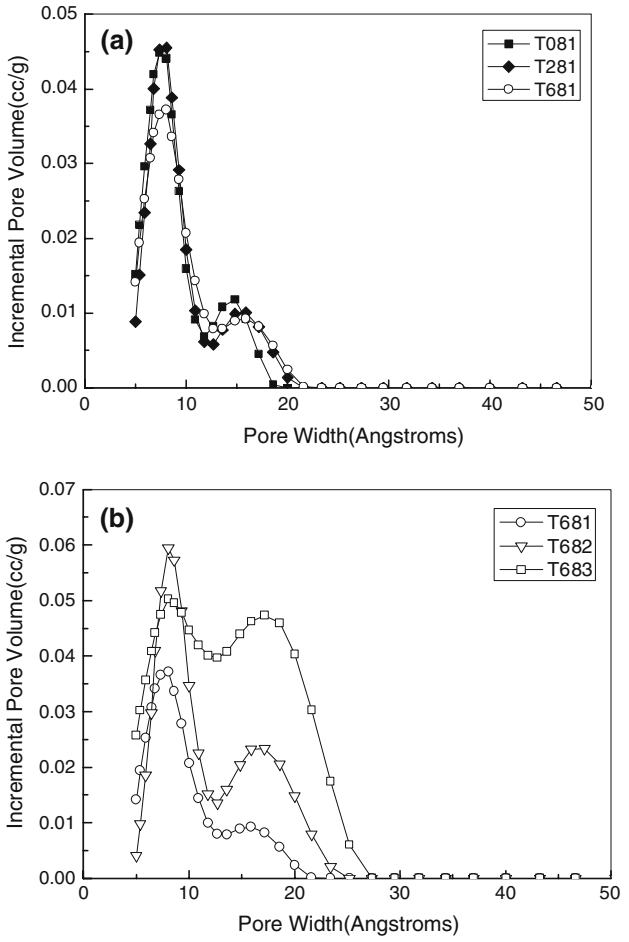

Fig. 3 Pore size distributions of the samples based on DFT theory (**a**) Effect of tension during stabilization; (**b**) Effect of the KOH concentration

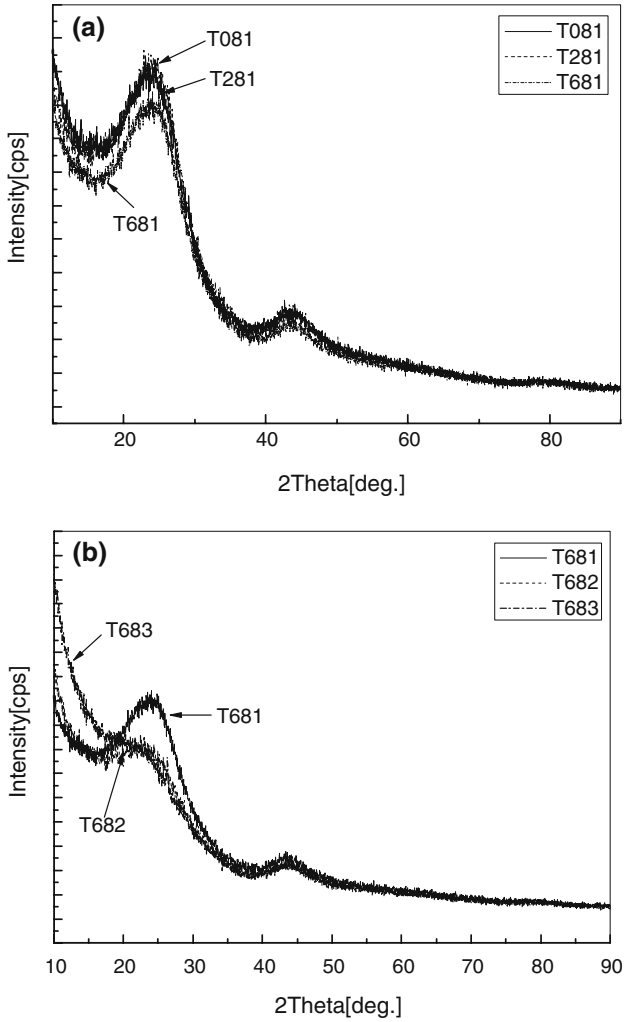

Fig. 4 X-ray diffraction of the samples: (**a**) Effect of tension during stabilization; (b) Effect of the KOH concentration

the KOH activation of the stabilized fibers. During KOH activation, the K ion was intercalated between the crystallite ribbons formed in the fiber axis and increased the inter-planar spacing.

According to KOH activation mechanism suggested by Otawa et al. [13] a considerable amount of metallic potassium was formed when activation temperature exceeded 700 °C. Potassium metal is considered to be formed by the reduction of K_2O by carbon at high temperatures. Potassium oxide (K_2O) is formed by the dehydration of KOH. Therefore, it was concluded that since the metallic potassium was mobile in the activation temperature, it was intercalated to the carbon matrix. As a result, several atomic layers of carbon were widened and were forming pores.

X-ray Photoelectron Spectroscopy (XPS)

Figure 5 shows the XPS survey spectra for the samples. Curve fitting [14] was optimized through the decomposition of C1s spectrum into five peaks: graphitic carbon (peak A, BE = 284.0 ~ 284.3 eV); carbon present in phenol, alcohol, ether, or C=N groups (peak B, BE = 285.3 ~ 285.7 eV); carbonyl or quinine groups (peak C, BE = 286.8 ~ 287.4 eV); carboxyl or ester groups (peak D, BE = 288.5 ~ 289.2), and; shake-up satellite peaks due to the π-π^* transitions in aromatic systems (peak E, BE = 290.2 ~ 291.1 eV). N1s spectra were fitted considering pyridinic, pyrrolic and quaternary nitrogen, and N-oxides. Peak A (BE = 398.0–398.1 eV) can be regarded as N-6 or pyridine structure; peak B (BE = 400.1–400.7 eV) corresponds to N-5, i.e., pyrrolic and/or pyridon-N moieties, peak C (BE = 401.4 ± 0.5 eV), to N-Q or quaternary nitrogen, and peak D (BE = 402–405 eV), to N-oxide.

During the stabilization, O/C and N/C were decreased for all samples. Similarly, during the KOH activation treatment for the stabilized fiber, the pyridine-like structure was decreased among the

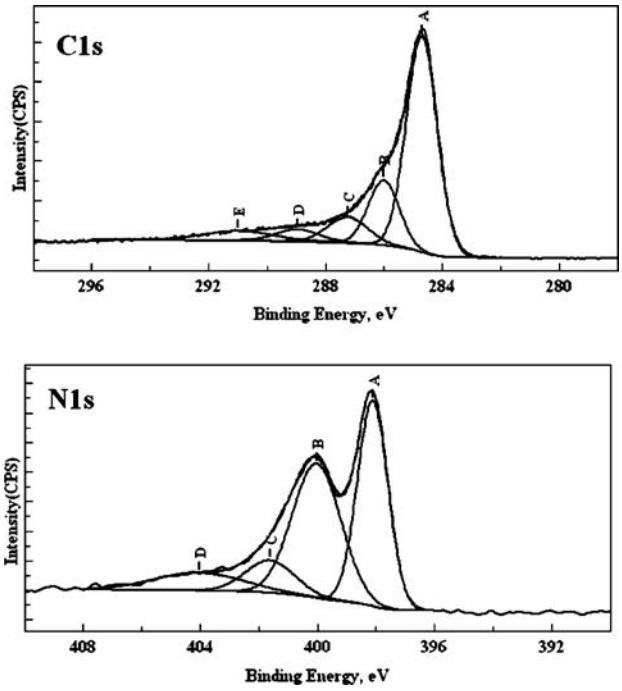

Fig. 5 XPS spectra of the samples

nitrogen superficial functional groups. The C=O was increased among the oxygen superficial functional groups. However, the carbonyl and carboxyl groups were decreased. Moreover, the samples showed the structure of the superficial functional group similar to that of XPS spectra in char and fiber using PAN as the raw material. This finding was consistent with the reports of previous researchers [14, 15].

Scanning Electron Microscopy (SEM)

The surface phenomena observed for PAN-ACFs under tension during stabilization did not exhibit significant changes as shown in Fig. 6. When PAN-ACF was activated under variation of KOH mole concentration, the serious surface damage occurred at 3 moles of KOH.

Electric conductivity

The electric conductivities of the PAN-ACFs under the pressure are shown in Fig. 7. Figure 7a shows the variations of electric conductivity under the tension during stabilization. The PAN-fiber was contracted in the direction of the fiber axis under the tension during stabilization. As a result, the density of the stabilized fiber could be increased and the electric conductivity was increased.

Figure 7b shows decreasing electric conductivity with increasing mole concentration of KOH due to the increased specific surface area with mole concentration of KOH solution. During the heat treatment of the stabilized fiber, a ladder structure was formed through a rearrangement of the polymer chain followed by the formation of an aromatic ring with graphite-like structure. Carbonized carbon at low temperature heat treatment exhibits the electric conductivity at room temperature due to the presence of non-carbon atoms such as oxygen, nitrogen, and other compositions [16–18]. Butkus and Yang [19] analyzed the process of electric conductivity in PAN carbon fiber on the cluster model of fiber consisting of carbon,

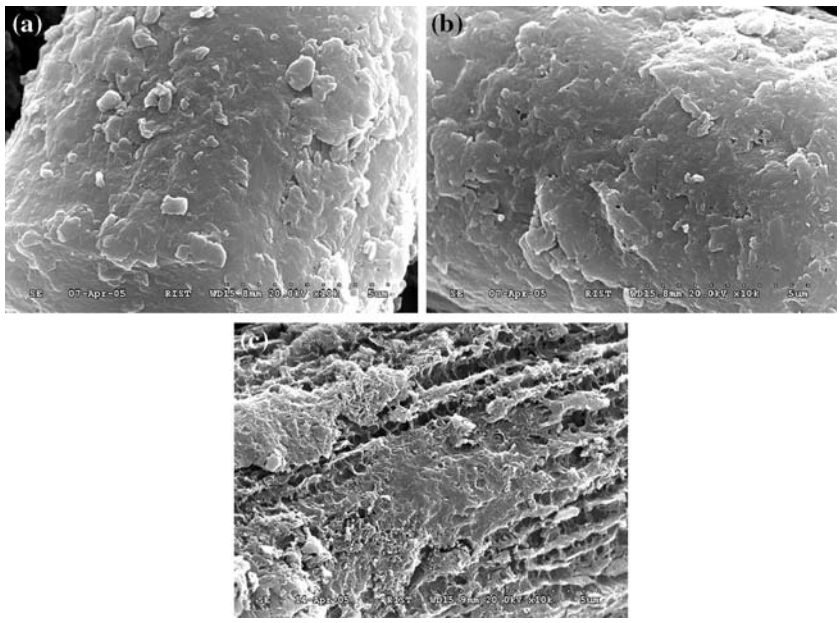

Fig. 6 Scanning electron microscopy: (**a**) T081; (**b**) T681; (**c**) T683

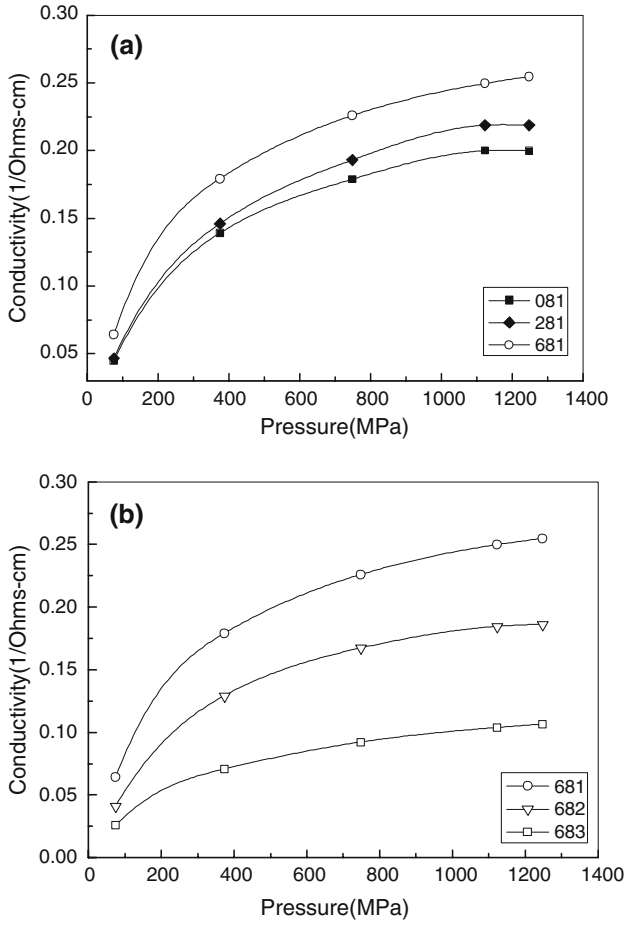

Fig. 7 Electric conductivity based on the pressure change of the samples (**a**) Effect of tension during stabilization; (**b**) Effect of the KOH concentration

nitrogen, and hydrogen atoms using the modified intermediate neglect of differential overlap (MINDO) molecular orbital (MO) method. The PAN carbon fiber heat-treated below 1000 °C was found to contain nitrogen within a graphite-like lattice. Therefore, the ''edge'' nitrogen site can be said to exhibit the same electron distribution as graphite. Since the content of non-carbon atoms was nearly constant for the PAN-ACFs prepared in this study, however, the difference in the electric conductivity between samples depends on the specific surface area and the pore size distribution rather than the presence of non-carbon atoms and superficial functional group. Moreover, less nitrogen and oxygen were present in T683. Given the large specific surface area compared with the other samples, it appears that the specific surface area significantly affects the electric conductivity.

Conclusion

The PAN-ACFs were prepared through the 1 M KOH activation treatment of PAN-fiber with varying tensions during the stabilization of PAN-fiber. The PAN-ACFs were also prepared through the 1, 2, 3 M KOH activation treatment of PAN- fiber at constant tension. The specific surface area and pore size distribution of the samples were affected by tensions applied during stabilization and KOH concentration during the activation treatment. The tension during stabilization increased the electric conductivity, which might be due to the molecular orientation along with the fiber axis. However, the electric conductivity decreased as the BET surface area increased. The electric conductivity of T681 had high value, which would be favorable for practical use in carbon electrode of EDLC.

Acknowledgement This work was supported by the Core Technology Development Program of the Ministry of Commerce, Industry and Energy (MOCIE). We are grateful for financial support.

References

1. Conway BE (1999) Electrochemical supercapacitors. Kluwer Academic/Plenum, New York
2. Conway BE (1991) J Electrochem Soc 138:1539
3. Sarangapani S, Tilak BV, Chen CP (1996) J Electrochem Soc 143:3791
4. Qu D, Shi H (1998) J Power Sources 74:99
5. Yang H, Yoshio M, Isono K, Kuramoto R (2002) Electrochem Solid State Lett 5:A141
6. Toyoda M, Tani Y, Soneda Y (2004) Carbon 42:2833
7. Kim Y, Horie Y, Matsuzawa Y, Ozaki S, Endo M, Dresselhaus M (2004) Carbon 42:2423
8. Zois H, Apekis L, Omastová M (2001) Macromol Symp 170:249
9. Brosseau C, Boulic F, Queffelec P, Bourbigot C, Mest YL, Loaec J (1997) J Appl Phys 81:882
10. Xiao M, Sun L, Liu J, Li Y, Gong K (2002) Polymer 43:2245
11. Brynauer S, Emmett PH, Teller E (1938) J Am Chem Soc 60:309
12. Donnet JB, Wang TK, Rebouillat S, Peng JCM (1998) Carbon fibers. Marcel Dekker, p 85
13. Otawa T, Yamada M, Tanibata R, Kawakami M (1990) Gas separation technology. Elsevier, New York, p 263
14. László K, Tombácz E, Josepovits K (2001) Carbon 39:1217
15. Pamula E, Rouxhet PG (2003) Carbon 41:1905
16. Jenkins GM, Kawakura J (1978) in Polymeric carbons. Cambridge University, Cambridge, p 90
17. Lerner NR (1981) J Appl Phys 52:6757
18. Gillespie DJ, Ehrlich AC (1992) J Non- Cryst Solids 144:231
19. Butkus AM, Yang CY (1981) Synth Metals 3:151